Progress In Electromagnetics Research M, Vol. 104, 199–212, 2021

A Novel Mirror Kirchhoff Approximation Method for Predicting the Shadowing Effect by a Metal Cuboid

Xin Du*, Kentaro Saito, Jun-ichi Takada, and Panawit Hanpinitsak

Abstract—This paper proposes an efficient and accurate scattered field prediction method based on Kirchhoff Approximation called 'Mirror Kirchhoff Approximation' (MKA) which is suitable for evaluating the shadowing effect by a metal cuboid. The disadvantages of conventional methods, such as low accuracy of Kirchhoff Approximation (KA) for metal cuboid and high computational complexity of Method of Moment (MoM) for a shadowing object at millimeter wave (mmWave), have motivated the establishment of an efficient and accurate prediction method for a metal cuboid at mmWave. The proposed method solves the previous issues by introducing the ray-based reflection into conventional KA. The idea and detail formulations of the proposed method are presented. The proposed method is validated by comparing with MoM and KA in terms of complexity and accuracy. The results imply that the proposed method presents good accuracy with low calculation time. The MKA has a maximum 8.3 dB improvement compared with conventional KA. Calculating time is improved by 67–915 times compared with MoM.

1. INTRODUCTION

With the spread of 5G, millimeter-wave (mmWave) band radio has come to be used for communication [1]. At mmWave, shadowing becomes more significant [2–4], and hence the prediction technique of the shadowing effect is needed.

To simulate the shadowing effect for an item of a small furniture or a vehicle, conventionally, full-wave simulation (e.g., Finite-Difference Time-Domain (FDTD) method [5], Method of Moment (MoM) [6] and its fast variant Multilevel Fast Multipole Algorithm (MLFMA) [7], and Finite Element Method (FEM) [8]) has been used. It solves Maxwell's Equation directly by a numerical approach, and hence it has good accuracy. However, it may call for unreasonable calculation time for large scale problems at mmWave since the object is very large compared with the wavelength, which significantly increases the number of meshes. Therefore, there is a need for a method based on high-frequency asymptotic approximation, which can reduce the computational complexity at mmWave. High-frequency asymptotic approximation can be divided into ray-based approximation (e.g., Geometrical Optics (GO) [9], Geometrical Theory of Diffraction (GTD) [10], and Uniform geometrical Theory of Diffraction (UTD) [11]) and source-based approximation (e.g., Physical Optics (PO) [12] and Kirchhoff Approximation (KA) [13]). These methods approximate the electromagnetic wave as combining several typical propagation phenomena such as incidence, reflection, diffraction, and scattering, and hence those methods can deal with large scattering problems within a reasonable calculation time.

In this research, a method based on KA for calculating the shadowing gain of a thick object is proposed. The reasons for selecting KA as the foundation are explained as follows. Firstly, KA is more suitable for the forward scattering problem [14] compared with PO, and hence it is expected to deal

Received 13 April 2021, Accepted 5 September 2021, Scheduled 19 September 2021

* Corresponding author: Xin Du (du.x.ab@m.titech.ac.jp).

The authors are with the Department of Transdisciplinary Science and Engineering, School of Environment and Society, Tokyo Institute of technology, Japan.

with the prediction of shadowing. Secondly, since the scattered field is obtained by integration over the lit region of the scattering surface in the source-based calculation [14], and KA can partially consider the geometrical shape of the shadowing object, unlike ray-based GO, GTD, and UTD. Thirdly, KA applying Fast Fourier Transform (FFT) or Inverse Fast Fourier Transform (IFFT) technique [15] is extremely fast as opposed to FDTD, MoM, and FEM. These advantages show that KA is a reasonable choice for further development.

However, the conventional KA has the accuracy issue to deal with a thick object. When KA predicts the forward scattering problem for a thick object, and the diffractions are counted by the integration of total field over the lit region of multi vacuum layers [16]. The diffraction wave is outstretched between the two layers, and the reflection from the shadowing object is always neglected [16]. That is the main accuracy issue of the conventional KA. Therefore, the restrictions of conventional methods have motivated the establishment of an accurate prediction method for evaluating the shadowing effect by a thick object with low calculation time.

Considering the aforementioned issues, this research aims to establish an efficient and accurate prediction method of shadowing effect by a metal cuboid, which can be approximated by an item of small furniture or a human body [17], at mmWave band. A novel method based on KA called 'Mirror Kirchhoff Approximation' (MKA) is proposed to achieve the goal.

The proposed MKA solves the accuracy issue of KA by introducing the reflection from an object into the diffraction of conventional KA. More details of the proposal and mathematical formulations are presented in Section 2.

Section 3 introduces the MoM simulation for validating the accuracy of the proposal. The details of the scenario, parameter setting, simulation environment are described.

Section 4 shows the simulation results of shadowing gain. Meanwhile, the calculation time is compared among the conventional KA, MoM, and proposed method.

Section 5 concludes this work, as well as the limitation of this method and the future work.

2. PROPOSAL AND FORMULATIONS

In this Section, the idea of the proposal will be introduced. The detailed mathematical formulations both in finite object height case and infinite object height case will be explained.

2.1. Conventional KA and Idea of Proposed MKA

The model of the proposal shown in Fig. 1 explains the idea in an easily understood manner. Initially, the location of a transmitter (Tx), receiver (Rx), and shadowing object is described as follows. A cuboid is considered as the shadowing object. Tx faces the front surface of the cuboid, and Rx faces the back surface of the cuboid. Tx and Rx are set at the same height. The z-axis parallel to the interior normal vector of the front surface is defined in a Cartesian coordinates system. The Tx-Rx line is set

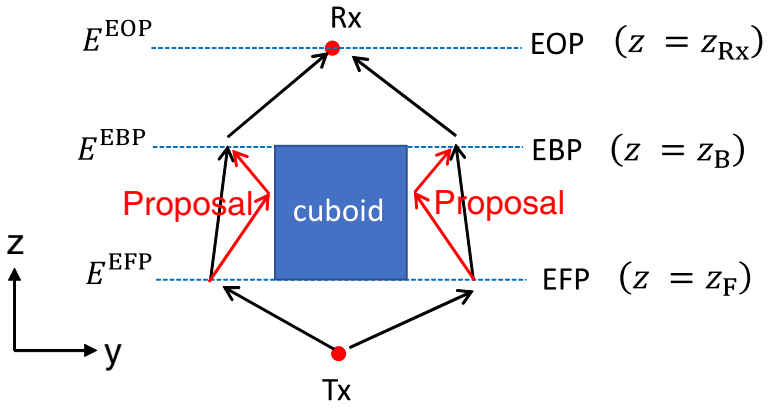

Figure 1. Model of proposal (y-z vertical view).

parallel to the z direction. Several geometric terminologies are defined as follows. The infinite large planes expanded from the front and back surfaces of the cuboid are defined as Expanded Front Plane (EFP) and Expanded Back Plane (EBP), respectively. Additionally, the infinite plane through Rx and paralleling to EFP or EBP is defined as Expanded Observation Plane (EOP). The plane equations of EFP, EBP, and EOP can be defined as $z = z_{\mathrm{F}}$, $z = z_{\mathrm{B}}$, and $z = z_{\mathrm{Rx}}$, respectively.

The use of conventional KA on those multi-planes for predicting the radio wave shadowed by an object is presented in [16]. To understand the issue of the conventional KA, a brief review is provided here. KA assumes that the total electric field on the shadowed region is zero. The total electric field on the lit region can be represented by the incident electric field only [13, 14]. The total electric fields $\mathbf{E}^{\mathrm{EFP}}(x, y, z_{\mathrm{F}})$ distributed on the first plane EFP everywhere can be determined by KA. Then, the scattered fields from this region can be obtained by the surface integration of induced current corresponding to the normal derivative of the total field [18]. Those scattered fields considered as secondary Huygens' sources propagate to the point (x, y, z_{B}) on the next plane EBP. By applying KA again, the total electric fields $\mathbf{E}^{\mathrm{EBP}}(x, y, z_{\mathrm{B}})$ distributed on EBP can be calculated. Repeating the approach in the same manner, the total electric fields $\mathbf{E}^{\mathrm{EOP}}(x, y, z_{\mathrm{Rx}})$ distributed on EOP can be calculated as well. The receiving electric field $\mathbf{E}^{\mathrm{Rx}}$ is identical to $\mathbf{E}^{\mathrm{EOP}}(x_{\mathrm{Rx}}, y_{\mathrm{Rx}}, z_{\mathrm{Rx}})$. Finally, the shadowing effect can be evaluated by comparing $\mathbf{E}^{\mathrm{Rx}}$ and the receiving electric field in free space.

It can be pointed out that the propagation wave in the above review is outstretched between the two planes, and the reflection effect from the shadowing object is neglected. This technique works well in [16] since [16] focuses on radio-wave propagation for suburban or a rural environment where instead of the reflection effect, the diffraction effect is dominant. However, the conventional KA always considers the shadowing object as an absorber, which may cause inaccuracy due to ignoring the shadowing object's real physical property. To compensate the deficiency, MKA is proposed in this work. Different from conventional KA, MKA considers the GO reflection effect that shadowing object reflects incident wave generated by the vacuum region of EFP to the vacuum region of EBP as shown in Fig. 1. By introducing ray-based GO into source-based KA calculation, the boundary condition corresponding to the real physical property of PEC can be satisfied. Since the introduction of GO reflection uses mirror image theory, this method is named 'Mirror Kirchhoff Approximation'.

2.2. Formulations in the Finite Object Height Case

The following procedures are proposed to establish MKA in the finite object height case. The first step is the calculation of fields distributed on the first plane EFP. To compute numerically, as shown in Fig. 2, the existence of field distributed on EFP, EBP, and EOP is truncated from the infinite large planes to the square aperture planes with the size of $T \times T$. The center of each aperture plane is identical to the projection of Tx onto EFP. The number of grids in each aperture plane is $M \times M$, where M is set to 2^l for employing FFT.

The spatial parameters x, y can be discretized by Eq. (1), where u, v are the discrete spatial indexes.

$$x = \frac{u}{M}T \quad (u = 0, 1, 2 \ldots, M-1) \quad , \quad y = \frac{v}{M}T \quad (v = 0, 1, 2 \ldots, M-1) \tag{1}$$

The time-harmonic incident electric field $\mathbf{E}^{\mathrm{Inc}}_{3\mathrm{D}}(u, v)$ at the point (u, v) on EFP from Tx based on KA is determined by Eqs. (2)–(13).

$$\mathbf{E}^{\mathrm{Inc}}_{3\mathrm{D}}(u, v) = \mathbf{E}_0 \times \frac{\lambda e^{-\mathrm{j}\mathbf{k}^{\mathrm{Inc}}(u,v)\cdot\mathbf{r}(u,v)}}{|\mathbf{r}(u, v)|} \tag{2}$$

where $\mathbf{E}_0$ is the electric field of the source with the direction depending on polarization. The magnitude of $\mathbf{E}_0$ can be arbitrary since the calculation of shadowing cancels $\mathbf{E}_0$ by Eq. (14). λ is the wavelength. $\mathbf{k}^{\mathrm{Inc}}(u, v)$ is the incident wave vector pointing to the point (u, v) on EFP. k is the wave number. $\mathbf{r}(u, v)$ is the distance vector pointing from Tx to the point (u, v) on EFP.

Assume that the set of all the points existing in the aperture of EFP excluding the front surface of the cuboid is A and that the set of all the points existing in the front surface of the cuboid is F. According to KA, the total electric fields distributed on an aperture of EFP $\mathbf{E}^{\mathrm{EFP}}(u, v)$ can be

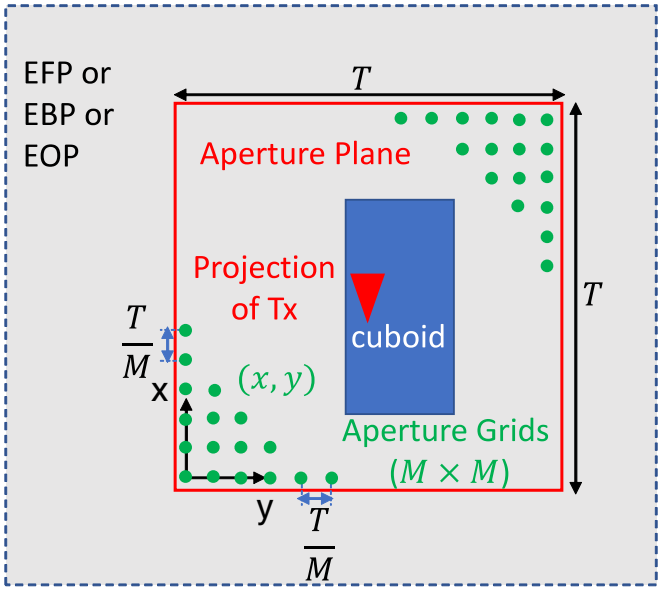

Figure 2. Aperture plane (x-y cross-section view).

determined by Eq. (3).

$$\mathbf{E}^{\mathrm{EFP}}(u,v) \approx \begin{cases} \mathbf{E}^{\mathrm{Inc}}_{\mathrm{3D}}(u,v) & (\text{for } (u,v) \in A) \\ 0 & (\text{for } (u,v) \in F) \end{cases} \tag{3}$$

The fields distributed on EBP and EOP can be determined by using vector potentials [18], and surface integration can be calculated by Ludwig numerical approach [19]. However, the complexity of vector potentials computing all the surface integrations determined by both the positions of source points on EFP and the positions of observation points on EBP is too much when the region of interest is large. It is more efficient to use the Angular Spectrum Method (ASM) [15, 20] by applying FFT for aperture plane since the complexity of computation can be reduced from $O(N^2)$ to $O(N \log_2 N)$, where N is the point number of one vacuum plane. ASM requires the fields to satisfy the homogeneous vector wave equation in the source-free region [20], while there is a shadowing object existing between EFP and EBP. The inhomogeneous region is needed to separate into several homogeneous regions by using the window function. Assume that the major propagation mechanisms are the diffraction from the left and right sides. Then, the left window region and right window region, where fields make a major contribution, are needed to be separated into two homogeneous regions as shown in Fig. 3.

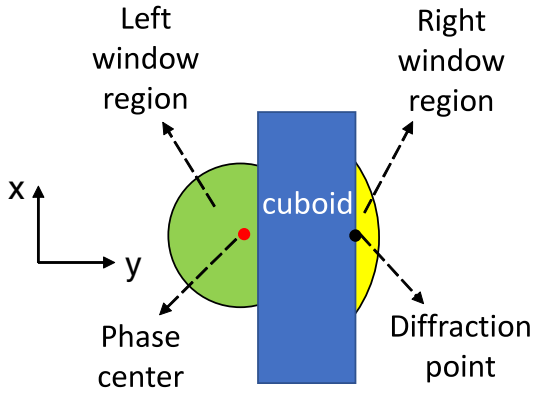

Figure 3. The region of window function (x-y cross-section view).

The implementation of window function based on the Fresnel Zone Number (FZN) [21] is for truncating the whole region to the major propagation mechanism region. FL, FR, BL, BR are defined as the abbreviations of left window region on EFP, right window region on EFP, left window region on EBP, and right window region on EBP, respectively. The region I (I =FL, FR, BL, BR) is created based on the Fresnel zone boundary. The window function $W^{\mathrm{I}}(u,v)$ for point (u,v) in the region I is determined by Eq. (4).

$$W^{\mathrm{I}}(u,v)=\begin{cases}\dfrac{1}{2}\left\{\cos\left(\dfrac{n_p^{\mathrm{I}}(u,v)-n_s^{\mathrm{I}}}{n_b^{\mathrm{I}}-n_s^{\mathrm{I}}}\pi\right)+1\right\} & (\text{for } (u,v)\in \mathrm{I})\\ 0 & (\text{otherwise})\end{cases}\qquad (\mathrm{I}=\mathrm{FL},\ \mathrm{FR},\ \mathrm{BL},\ \mathrm{BR}) \tag{4}$$

where $n_p^{\mathrm{I}}(u,v)$ denotes the FZN of point (u,v) in the region I. n_b^{I} denotes the FZN of the window boundary of the region I. n_s^{I} denotes the FZN of the stationary point in the region I. For the NLoS case, the stationary points are two diffraction points for both sides. For the LoS case, the stationary points are a phase center for one side and a diffraction point for another side. The definition of NLoS or LoS is whether the phase center is inside the cuboid or not. The phase center means the point which is the intersection between the Tx-Rx line and front of the cuboid. The size of window for the region I is determined by the value of $\Delta n=n_b^{\mathrm{I}}-n_s^{\mathrm{I}}$.

The electric fields $\mathbf{E}^{\mathrm{FL}}(u,v)$, $\mathbf{E}^{\mathrm{FR}}(u,v)$ distributed on FL and FR, respectively, can be calculated by Eq. (5).

$$\mathbf{E}^{\mathrm{FL}}(u,v)=W^{\mathrm{FL}}(u,v)\times\mathbf{E}^{\mathrm{EFP}}(u,v)\quad ,\quad \mathbf{E}^{\mathrm{FR}}(u,v)=W^{\mathrm{FR}}(u,v)\times\mathbf{E}^{\mathrm{EFP}}(u,v) \tag{5}$$

The second step is the calculation of fields distributed on the second plane EBP by ASM. Applying 2D IFFT, each component of the fields $\mathbf{E}^{\mathrm{FL}}(u,v)$ and $\mathbf{E}^{\mathrm{FR}}(u,v)$ can be decomposed to angular-spectrum-varying plane waves by Eq. (6).

$$\begin{pmatrix}C_x^{\mathrm{FL}}(p,q) & C_x^{\mathrm{FR}}(p,q)\\ C_y^{\mathrm{FL}}(p,q) & C_y^{\mathrm{FR}}(p,q)\end{pmatrix}=\frac{1}{4\pi^2}\sum_{u=0}^{M-1}\sum_{v=0}^{M-1}\begin{pmatrix}E_x^{\mathrm{FL}}(u,v) & E_x^{\mathrm{FR}}(u,v)\\ E_y^{\mathrm{FL}}(u,v) & E_y^{\mathrm{FR}}(u,v)\end{pmatrix}e^{\mathrm{j}2\pi\left(\frac{up+vq}{M}\right)}\left(\frac{T}{M}\right)^2 \tag{6}$$

where $E_x^{\mathrm{FL}}(u,v)$, $E_y^{\mathrm{FL}}(u,v)$ are the x,y-components of $\mathbf{E}^{\mathrm{FL}}(u,v)$, respectively. $E_x^{\mathrm{FR}}(u,v)$, $E_y^{\mathrm{FR}}(u,v)$ are the x,y-components of $\mathbf{E}^{\mathrm{FR}}(u,v)$, respectively. $C_x^{\mathrm{FL}}(p,q)$, $C_y^{\mathrm{FL}}(p,q)$, $C_x^{\mathrm{FR}}(p,q)$, $C_y^{\mathrm{FR}}(p,q)$ are the weighting coefficients of $E_x^{\mathrm{FL}}(u,v)$, $E_y^{\mathrm{FL}}(u,v)$, $E_x^{\mathrm{FR}}(u,v)$, $E_y^{\mathrm{FR}}(u,v)$, respectively. p, q are the discrete frequency spectral indexes from $1-\frac{M}{2}$ to $\frac{M}{2}$.

Applying 2D FFT, those plane waves propagating along z direction with a propagation distance of $z'=z_{\mathrm{B}}-z_{\mathrm{F}}$ are superposed as secondary incident fields for EBP by Eqs. (7)–(8).

$$\begin{pmatrix}E_x^{\mathrm{BL}}(u,v) & E_x^{\mathrm{BR}}(u,v)\\ E_y^{\mathrm{BL}}(u,v) & E_y^{\mathrm{BR}}(u,v)\end{pmatrix}=\sum_{p=1-\frac{M}{2}}^{\frac{M}{2}}\sum_{q=1-\frac{M}{2}}^{\frac{M}{2}}\begin{pmatrix}C_x^{\mathrm{FL}}(p,q) & C_x^{\mathrm{FR}}(p,q)\\ C_y^{\mathrm{FL}}(p,q) & C_y^{\mathrm{FR}}(p,q)\end{pmatrix}e^{-\mathrm{j}\left\{2\pi\left(\frac{up+vq}{M}\right)+k_{\mathrm{z}}z'\right\}}\left(\frac{2\pi}{T}\right)^2 \tag{7}$$

$$k_{\mathrm{z}}=\begin{cases}+\sqrt{k^2-\left(\dfrac{2\pi}{T}p\right)^2-\left(\dfrac{2\pi}{T}q\right)^2} & \left(\text{for } k^2\geq\left(\dfrac{2\pi}{T}p\right)^2+\left(\dfrac{2\pi}{T}q\right)^2\right)\\ -\mathrm{j}\sqrt{\left(\dfrac{2\pi}{T}p\right)^2+\left(\dfrac{2\pi}{T}q\right)^2-k^2} & \left(\text{for } k^2<\left(\dfrac{2\pi}{T}p\right)^2+\left(\dfrac{2\pi}{T}q\right)^2\right)\end{cases} \tag{8}$$

where $E_x^{\mathrm{BL}}(u,v)$, $E_y^{\mathrm{BL}}(u,v)$ are the x,y-components of incident field $\mathbf{E}^{\mathrm{BL}}(u,v)$ at point (u,v) on EBP, which is the superposition of the fields scattered by all the points of FL. $E_x^{\mathrm{BR}}(u,v)$, $E_y^{\mathrm{BR}}(u,v)$ are the x,y-components of incident field $\mathbf{E}^{\mathrm{BR}}(u,v)$ at point (u,v) on EBP, which is the superposition of the fields scattered by all the points of FR. k_{z} represents spectral frequency parameters for z domain. There is no need to calculate z-component of $\mathbf{E}^{\mathrm{BL}}(u,v)$ and $\mathbf{E}^{\mathrm{BR}}(u,v)$ since $E_{\mathrm{z}}^{\mathrm{BL}}(u,v)$ and $E_{\mathrm{z}}^{\mathrm{BR}}(u,v)$ are zero for propagating along z direction.

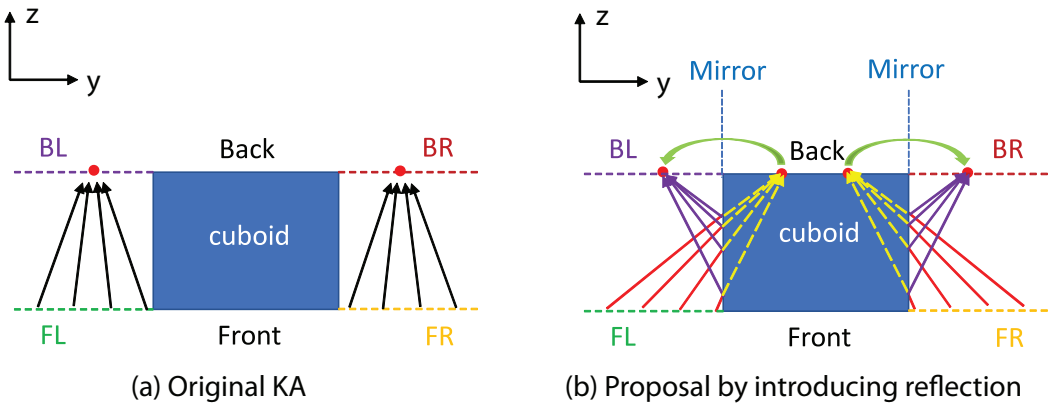

Figure 4. The establishment of mirror Kirchhoff approximation (y-z vertical view).

Based on the conventional KA which only considers the source from EFP as shown in Fig. 4(a), the proposed MKA introduces reflection rays from shadowing object by using mirror image theory as shown in Fig. 4(b). The proposed MKA calculates the total electric fields $\mathbf{E}^{\mathrm{EBP}}(u,v)$ distributed on EBP by Eq. (9).

$$\mathbf{E}^{\mathrm{EBP}}(u,v) \approx \begin{cases} W^{\mathrm{BL}}(u,v)\times(\mathbf{E}^{\mathrm{BL}}(u,v) + R\mathbf{E}^{\mathrm{BL}}(u,2[v_{\mathrm{L}}]-v)) & (\text{for } (u,v)\in \mathrm{BL}) \\ W^{\mathrm{BR}}(u,v)\times(\mathbf{E}^{\mathrm{BR}}(u,v) + R\mathbf{E}^{\mathrm{BR}}(u,2[v_{\mathrm{R}}]-v)) & (\text{for } (u,v)\in \mathrm{BR}) \\ 0 & (\text{otherwise}) \end{cases} \tag{9}$$

where R represents the reflection coefficient. For metal case, $R=-1$. $[v_{\mathrm{L}}]$ is the discrete index corresponding to spatial parameter y_{L} which is calculated by Eq. (1), where [.] is the round function to the nearest integer. $[v_{\mathrm{R}}]$ is the discrete index corresponding to spatial parameter y_{R}. $\mathbf{E}^{\mathrm{BL}}(u,2[v_{\mathrm{L}}]-v)$ is the image field of $\mathbf{E}^{\mathrm{BL}}(u,v)$ by considering left side of cuboid as a mirror. $\mathbf{E}^{\mathrm{BR}}(u,2[v_{\mathrm{R}}]-v)$ is the image field of $\mathbf{E}^{\mathrm{BR}}(u,v)$ by considering right side of cuboid as a mirror.

The third step is the calculation of fields distributed on the third plane EOP based on ASM again. This time, the separation of field distribution is not needed since the region between EBP and EOP is homogeneous. On the EOP, the total electric fields $\mathbf{E}^{\mathrm{EOP}}(u,v)$ based on the conventional KA approach, and the total electric fields $\mathbf{E}^{\mathrm{EOP}}(u,v)$ based on the proposed MKA approach, are determined by Eqs. (10)–(11).

$$\begin{pmatrix} C_x^{\mathrm{EBP}}(p,q) \\ C_y^{\mathrm{EBP}}(p,q) \end{pmatrix} = \frac{1}{4\pi^2}\sum_{u=0}^{M-1}\sum_{v=0}^{M-1}\begin{pmatrix} E_x^{\mathrm{EBP}}(u,v) \\ E_y^{\mathrm{EBP}}(u,v) \end{pmatrix} e^{\mathrm{j}2\pi(\frac{up+vq}{M})}\left(\frac{T}{M}\right)^2 \tag{10}$$

$$\begin{pmatrix} E_x^{\mathrm{EOP}}(u,v) \\ E_y^{\mathrm{EOP}}(u,v) \end{pmatrix} = \sum_{p=1-\frac{M}{2}}^{\frac{M}{2}}\sum_{q=1-\frac{M}{2}}^{\frac{M}{2}}\begin{pmatrix} C_x^{\mathrm{EBP}}(p,q) \\ C_y^{\mathrm{EBP}}(p,q) \end{pmatrix} e^{-\mathrm{j}\left\{2\pi(\frac{up+vq}{M})+k_z z''\right\}}\left(\frac{2\pi}{T}\right)^2 \tag{11}$$

where $E_x^{\mathrm{EBP}}(u,v)$, $E_y^{\mathrm{EBP}}(u,v)$ are the x,y-components of $\mathbf{E}^{\mathrm{EBP}}(u,v)$. $E_x^{\mathrm{EOP}}(u,v)$, $E_y^{\mathrm{EOP}}(u,v)$ are the x,y-components of $\mathbf{E}^{\mathrm{EOP}}(u,v)$. $C_x^{\mathrm{EBP}}(p,q)$ and $C_y^{\mathrm{EBP}}(p,q)$ are the weighting coefficients of $E_x^{\mathrm{EBP}}(u,v)$ and $E_y^{\mathrm{EBP}}(u,v)$, respectively. $z''=z_{\mathrm{Rx}}-z_{\mathrm{B}}$ is the propagation distance between EBP and EOP.

The receiving electric field $\mathbf{E}^{\mathrm{Rx}}$ at Rx is determined by Eq. (12).

$$\mathbf{E}^{\mathrm{Rx}} = \mathbf{E}^{\mathrm{EOP}}([u_{\mathrm{Rx}}],[v_{\mathrm{Rx}}]) \tag{12}$$

where $[u_{\mathrm{Rx}}]$, $[v_{\mathrm{Rx}}]$ are discrete indexes corresponding to coordinate of Rx point.

The total receiving electric field in free space $\mathbf{E}_{\mathrm{3D}}^{\mathrm{Free}}$ is determined by Eq. (13).

$$\mathbf{E}_{\mathrm{3D}}^{\mathrm{Free}} = \mathbf{E}_0 \times \frac{\lambda e^{-\mathrm{j}kd}}{d} \tag{13}$$

where d is the distance between Tx and Rx.

The shadowing gain $\mathrm{SG}_{3\mathrm{D}}$ is determined by Eq. (14).

$$\mathrm{SG}_{3\mathrm{D}} = 20\log_{10}\frac{|\mathbf{E}^{\mathrm{Rx}}|}{|\mathbf{E}^{\mathrm{Free}}_{3\mathrm{D}}|} \quad [\mathrm{dB}] \tag{14}$$

2.3. Formulations in the Infinite Object Height Case

If the object has infinite height, the 3D problem can be simplified to the 2D problem. The 3D cuboid can be considered as a rectangular plane in y-z plane, and the spatial variable u can be absent since the whole environment in x direction is uniform. Since the same procedures for the general case of polarization have already been explained in Section 2.2, here only a special case of the perpendicular polarization is focused to explain the difference between 2D formulation and 3D formulation for the sake of simplicity. In perpendicular polarization, only x-component of electric field works, and hence the vector equations can be simplified to scalar equations. An electric line source with the cylindrical wave is considered as Tx. Equations (2) can be replaced by Eq. (15).

$$E^{\mathrm{Inc}}_{2\mathrm{D}}(v) = -\frac{k^2 I_0}{4\omega\epsilon}H^{(2)}_0(k\rho(v)) \tag{15}$$

where $E^{\mathrm{Inc}}_{2\mathrm{D}}(u)$ is the z-component of incident field arriving at point (v) on EFP in infinite object height case. $E^{\mathrm{Free}}_{2\mathrm{D}}$ is the z-component of incident field arriving at Rx in infinite object height case. I_0 is the magnitude of electric field of source, and it can be arbitrary since the calculation of shadowing cancels I_0 by Eq. (22). ω is the angular frequency. ϵ is the permittivity of vacuum. $\rho(v)$ is the distance vector pointing from Tx to point (v) on EFP. $H^{(2)}_0(.)$ represents the second kind of Hankel function for 0 order.

In the ASM calculation, instead of 2D IFFT and 2D FFT, only the 1D IFFF and 1D FFT are needed. Eqs. (6)–(8) and (10)–(11) can be replaced by Eqs. (16)–(18) and (19)–(20).

$$\begin{pmatrix} C^{\mathrm{FL}}_x(q) & C^{\mathrm{FR}}_x(q) \end{pmatrix} = \frac{1}{2\pi}\sum_{v=0}^{M-1}\begin{pmatrix} E^{\mathrm{FL}}_x(v) & E^{\mathrm{FR}}_x(v) \end{pmatrix} e^{\mathrm{j}2\pi\left(\frac{vq}{M}\right)}\left(\frac{T}{M}\right) \tag{16}$$

$$\begin{pmatrix} E^{\mathrm{BL}}_x(v) & E^{\mathrm{BR}}_x(v) \end{pmatrix} = \sum_{q=1-\frac{M}{2}}^{\frac{M}{2}}\begin{pmatrix} C^{\mathrm{FL}}_x(q) & C^{\mathrm{FR}}_x(q) \end{pmatrix} e^{-\mathrm{j}\left\{2\pi\left(\frac{vq}{M}\right)+k_{\mathrm{z}}z'\right\}}\left(\frac{2\pi}{T}\right) \tag{17}$$

$$k_{\mathrm{z}} = \begin{cases} +\sqrt{k^2-\left(\dfrac{2\pi}{T}q\right)^2} & \left(\text{for } \; k^2 \geq \left(\dfrac{2\pi}{T}q\right)^2\right) \\ -\mathrm{j}\sqrt{\left(\dfrac{2\pi}{T}q\right)^2-k^2} & \left(\text{for } \; k^2 < \left(\dfrac{2\pi}{T}q\right)^2\right) \end{cases} \tag{18}$$

$$C^{\mathrm{EBP}}_x(q) = \frac{1}{2\pi}\sum_{v=0}^{M-1}E^{\mathrm{EBP}}_x(v)e^{\mathrm{j}2\pi\left(\frac{vq}{M}\right)}\left(\frac{T}{M}\right) \tag{19}$$

$$E^{\mathrm{EOP}}_x(v) = \sum_{q=1-\frac{M}{2}}^{\frac{M}{2}}C^{\mathrm{EBP}}_x(q)e^{-\mathrm{j}\left\{2\pi\left(\frac{vq}{M}\right)+k_{\mathrm{z}}z''\right\}}\left(\frac{2\pi}{T}\right) \tag{20}$$

For the final step in the infinite object height case, the total field in free space $E^{\mathrm{Free}}_{2\mathrm{D}}$ and the shadowing gain $\mathrm{SG}_{2\mathrm{D}}$ are determined by Eqs. (21) and (22).

$$E^{\mathrm{Free}}_{2\mathrm{D}} = -\frac{k^2 I_0}{4\omega\epsilon}H^{(2)}_0(kd) \tag{21}$$

$$\mathrm{SG}_{2\mathrm{D}} = 20\log_{10}\frac{|E^{\mathrm{Rx}}|}{|E^{\mathrm{Free}}_{2\mathrm{D}}|} \quad [\mathrm{dB}] \tag{22}$$

3. SIMULATION

For validating the accuracy of conventional KA and proposed MKA, full-wave MoM was simulated. However, for the scattering problem of an object in 3D space at mmWave, the validating time of MoM was unreasonable. Therefore, the validation by 2D MoM was considered to reduce the validating time. Thus a cuboid with infinite height was considered as a shadowing object for the sake of simplicity. The perpendicular polarization was considered for all the methods.

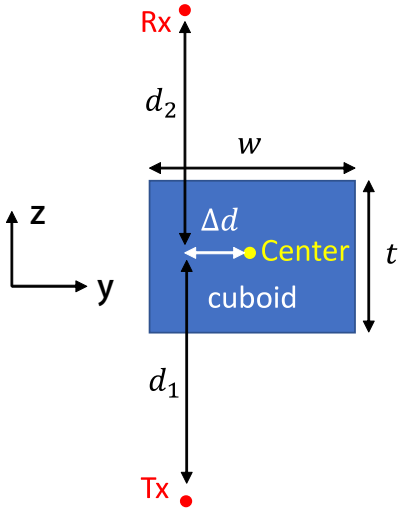

Figure 5. The environment of simulation (y-z vertical view).

As shown in Fig. 5, the scenario of the simulation was explained as follows. An open region was considered as the environment, where there were only Tx, Rx, and a cuboid. The parameters of the environment are shown in Table 1. w denotes the width of the cuboid. t denotes the thickness of the cuboid. d_1 denotes the distance between the center of the cuboid and Tx. d_2 denotes the distance between the center of the cuboid and Rx. f denotes frequency of simulation. Δd denotes the distance between the center of the cuboid and Tx-Rx line. Δd was changed from -45λ m to 0 m with an interval of 0.1λ m. $\Delta d < 0$ meant cuboid was located at the left side of the Tx-Rx line. $\Delta d > 0$ meant cuboid was located at the right side of the Tx-Rx line. t was changed from 0.001 m to 0.3 m with an interval of 0.001 m. f was changed from 17 GHz to 66.5 GHz with an interval of 0.5 GHz. The parameters of KA and MKA are shown in Table 2.

Table 1. Environment parameter.

Parameter	Value
f (GHz)	17 : 0.5 : 66.5
d_1 (m)	2
d_2 (m)	8
w (m)	0.5
t (m)	0.001 : 0.001 : 0.3
Δd (λ)	-45 : 0.1 : 0

The parameter setting of KA and MKA is described as follows. The window size was set by confirming the convergence of results. The aperture plane should be large enough for including the whole surface of the shadowing object and ensuring a good resolution of frequency spectral parameters [15]. Grid interval should not be larger than half wavelength according to sampling theory [22]. Grid interval

Table 2. KA and MKA parameter.

Parameter	Value
Number of grid points M	2^{17}
Grid interval (m)	0.1λ
Window size Δn	19

determined the distance interval, and hence the requirement of high distance resolution increased grid points on the large aperture. This meant that the computational complexity was increased. The above parameter setting considered the balance between accuracy and computation memory.

To validate the accuracy of KA and MKA, MoM [23] was simulated. The piecewise constant function was selected as the basis function. MoM with point matching method was implemented by using MATLAB. The implemented MoM was validated by the canonical problems [18]. To obtain the convergence result, the mesh size was set to $\frac{\lambda}{10}$, and there were 25 integration points for each mesh.

4. RESULTS AND DISCUSSION

Firstly, when the thickness was fixed, the frequency was fixed at 66.5 GHz, and the distance was changed. The shadowing gain results of KA, MKA,and MoM are shown in Fig. 6–Fig. 9 for $t = 0.01$ m, $t = 0.03$ m, $t = 0.1$ m, and $t = 0.3$ m, respectively. The horizontal axis was Δd (m) introduced in Fig. 5. The vertical axis was shadowing gain result in decibel (dB) scale.

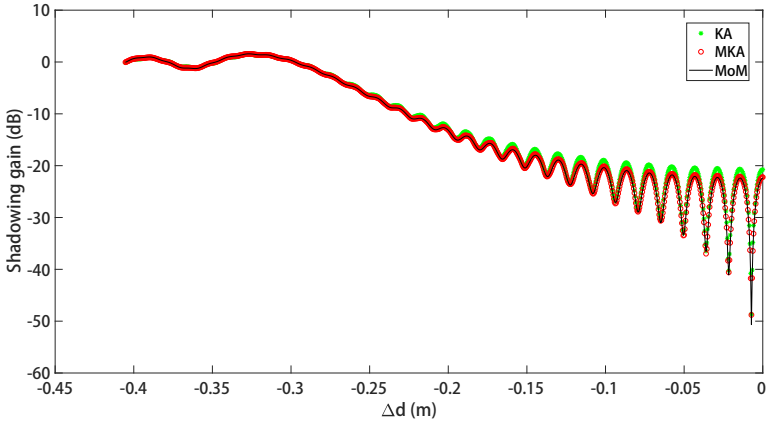

Figure 6. The plot of distance and shadowing gain for $t = 0.01$ m and $f = 66.5$ GHz.

From the results, for each case, the proposed MKA was in good agreement with MoM. The improvement of the proposal was validated by comparing it with conventional KA and MoM. Additionally, it could be found that as the thickness of the cuboid increases, the improvement becomes more significant.

Secondly, when the distance was fixed at 0 m, the frequency was fixed at 66.5 GHz, and the thickness was changed. The relationship between thickness and shadowing gain is shown in Fig. 10. The horizontal axis was t (m) introduced in Fig. 5.

From the result, the proposed method provided good prediction results for the object with any thickness. The reflection in the secondary diffraction became larger and larger with increasing thickness. For the case of $f = 66.5$ GHz, $\Delta d = 0$ m, and $t = 0.3$ m, the proposed MKA had 8.3 dB improvement compared with conventional KA.

Thirdly, when the distance was fixed at 0 m, the thickness was fixed at 0.3 m, and the frequency was changed from 17 GHz to 66.5 GHz. The relationship between frequency and shadowing gain is shown

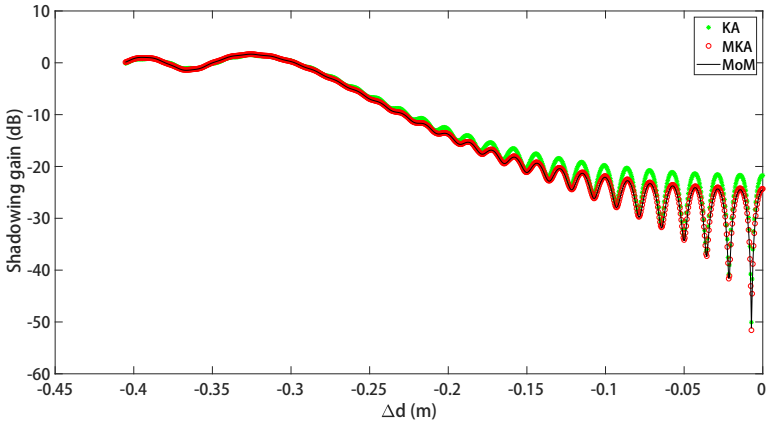

Figure 7. The plot of distance and shadowing gain for $t = 0.03\,\mathrm{m}$ and $f = 66.5\,\mathrm{GHz}$.

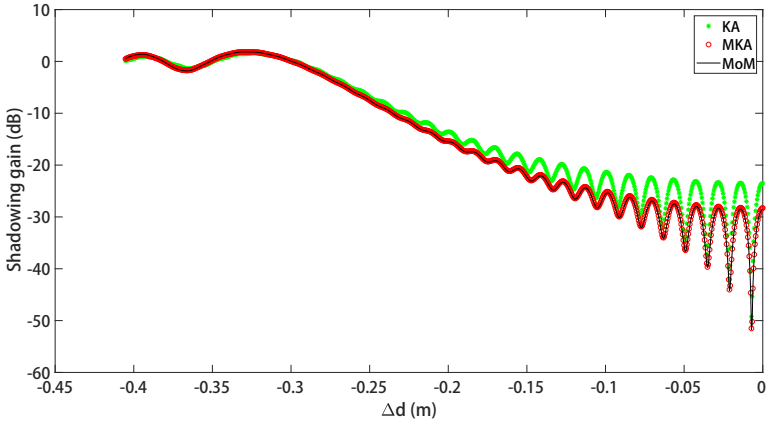

Figure 8. The plot of distance and shadowing gain for $t = 0.1\,\mathrm{m}$ and $f = 66.5\,\mathrm{GHz}$.

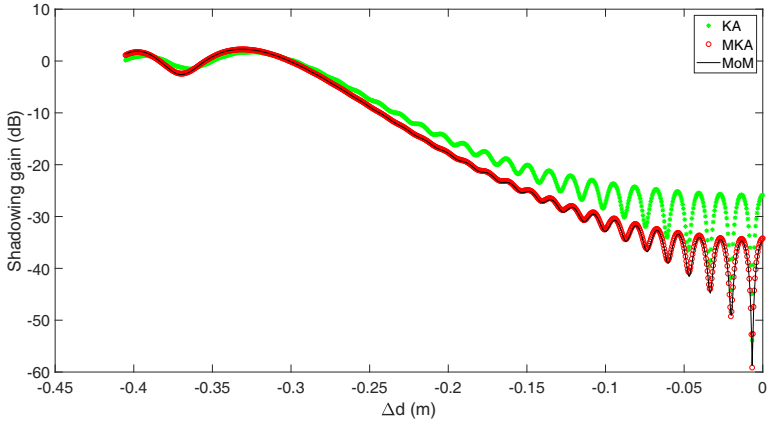

Figure 9. The plot of distance and shadowing gain for $t = 0.3\,\mathrm{m}$ and $f = 66.5\,\mathrm{GHz}$.

in Fig. 11.

From the result, the proposed method provided good prediction results for the object with any frequency. The reflection in the secondary diffraction became larger and larger with increasing frequency. The frequency characteristics of shadowing can be predicted by MKA.

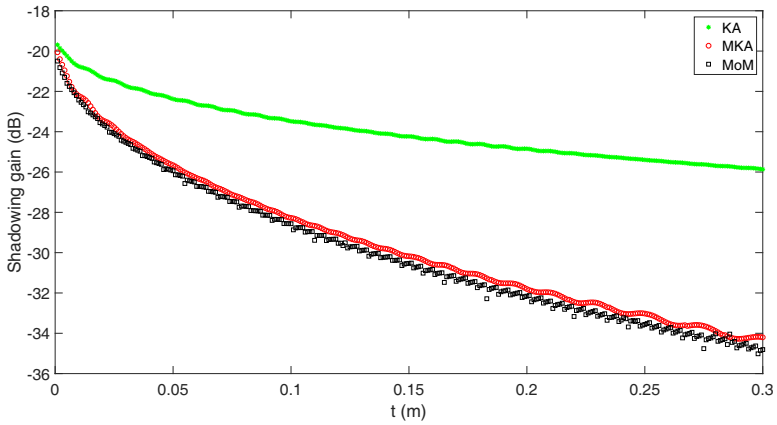

Figure 10. The relation between thickness and shadowing gain for $\Delta d = 0\,\text{m}$ and $f = 66.5\,\text{GHz}$.

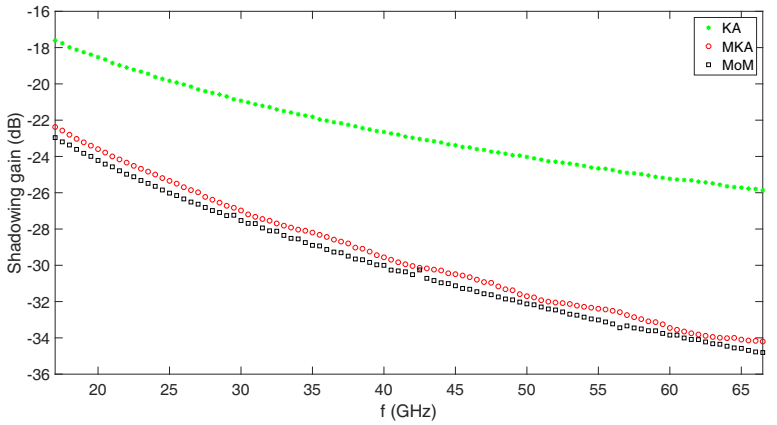

Figure 11. The relation between frequency and shadowing gain for $\Delta d = 0\,\text{m}$ and $t = 0.3\,\text{m}$.

Furthermore, the calculation time was compared among the KA, MKA, and MoM. The platform of calculating computer was Windows 10 Home. The processor of calculating computer was Intel(R) Core(TM) i7-8750H CPU @ 2.20 GHz. The usable installed memory of the calculating computer was 15.8 GB. The system type of calculating computer was 64-bit Operating System, x64-based processor. The simulation software was MATLAB. The result of the relation between thickness and calculation time is shown in Fig. 12 for $\Delta d = 0\,\text{m}$ and $f = 66.5\,\text{GHz}$. The result of the relation between frequency and calculation time is shown in Fig. 13 for $\Delta d = 0\,\text{m}$ and $t = 0.3\,\text{m}$. The vertical axis is calculation time (s) on a logarithmic scale.

The calculation time of the conventional KA was about 0.08 s for any thickness or frequency. The calculation time of the proposed MKA was about 0.21 s for any thickness or frequency. The calculation time of MoM was about from 82.45 s to 192.12 s for increasing thickness at $f = 66.5\,\text{GHz}$ and from 14.07 s to 192.12 s for increasing frequency at $t = 0.3\,\text{m}$. Compared with full-wave MoM, the MKA could provide an extremely fast calculation speed. The errors of the accuracies were evaluated by considering MoM as a reference and calculated by Eq. (23).

$$\epsilon = \left| \frac{\text{SG}_{\text{Method}} - \text{SG}_{\text{MoM}}}{\text{SG}_{\text{MoM}}} \right| \tag{23}$$

where ϵ means the error of the accuracy. SG_{MoM} means the shadowing gain calculated by MoM in dB scale. $\text{SG}_{\text{Method}}$ means the shadowing gain calculated by KA, MKA, or MoM in dB scale.

The comparisons of the error of the accuracy and computational time among the proposed method

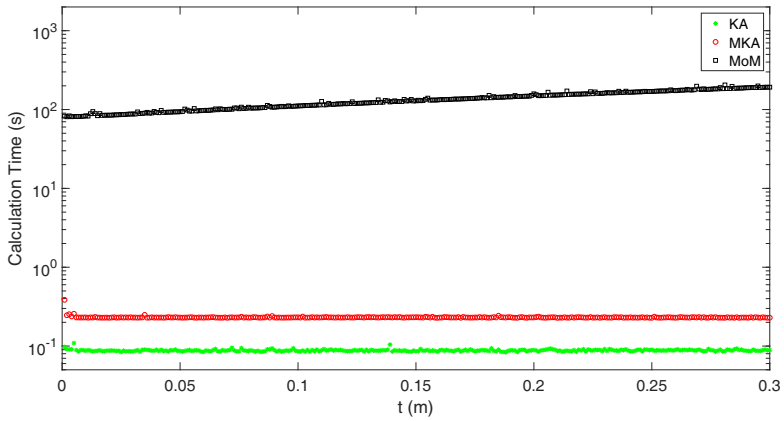

Figure 12. The relation between thickness and calculation time for $\Delta d = 0\,\mathrm{m}$ and $f = 66.5\,\mathrm{GHz}$.

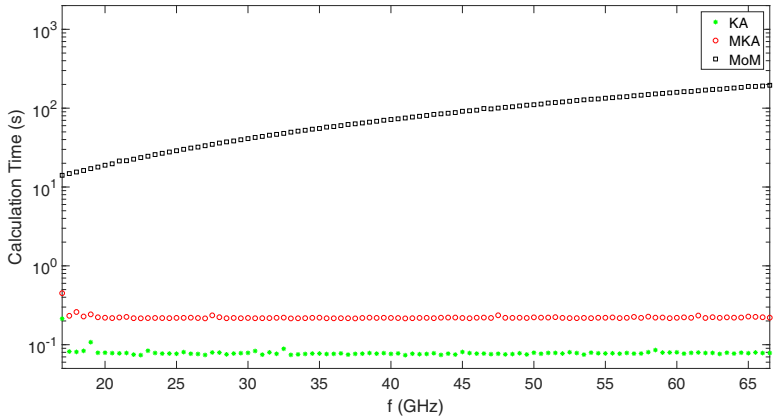

Figure 13. The relation between frequency and calculation time for $\Delta d = 0\,\mathrm{m}$ and $t = 0.3\,\mathrm{m}$.

and conventional methods are shown in Table 3 and Table 4. Table 3 is for the condition of changing thickness at $\Delta d = 0\,\mathrm{m}$ and $f = 66.5\,\mathrm{GHz}$. Table 4 is for the condition of changing frequency at $\Delta d = 0\,\mathrm{m}$ and $t = 0.3\,\mathrm{m}$.

Table 3. Comparison of proposed method and conventional methods for $\Delta d = 0\,\mathrm{m}$ and $f = 66.5\,\mathrm{GHz}$.

Method	Error	Computational time (s)
KA	$3.9\% \sim 26.3\%$	0.08
MoM	0%	$82.45 \sim 192.12$
This work	$0.3\% \sim 3.2\%$	0.21

Table 4. Comparison of proposed method and conventional methods for $\Delta d = 0\,\mathrm{m}$ and $t = 0.3\,\mathrm{m}$

Method	Error	Computational time (s)
KA	$23.1\% \sim 25.8\%$	0.08
MoM	0%	$14.07 \sim 192.12$
This work	$0.3\% \sim 2.7\%$	0.21

From Table 3 and Table 4, the proposed method had a good balance between accuracy and calculation time. Through reduced computational time, this technique was practical for 5G mobile shadowing prediction in a large environment. This paper focuses on one shadowing object, while the proposed technique could be utilized in multiple objects case by applying multiple extended planes. The metal cuboid could be approximated by furniture including a refrigerator, air conditioner, or any electrical device with a cuboid shape. In addition to mobile use, the car could also be considered as a cuboid which might be applied in the autopilot field.

5. CONCLUSION

In this paper, a novel method MKA for predicting the shadowing effect by cuboid has been proposed. The idea by introducing ray-based GO into source-based KA was presented. The detailed mathematical formulations of the proposal were explained. The MoM was used as a reference for validating the proposed method. From the validating result, the proposed MKA presented a good balance between accuracy and calculation time. The MKA had a maximum 8.3 dB improvement compared with conventional KA. Calculating time was improved by 67–915 times compared with MoM. Furthermore, the use case of the proposal was discussed.

As the limitation of this work, MKA currently cannot deal with a curved surface. To solve this drawback, the approximation of curved surface by the combination of several cuboids is considered for future study. The extension of the applicable range is a future topic.

REFERENCES

1. ITU-R, *Use of the Frequency Band 66–71 GHz for International Mobile Telecommunications and Coexistence with Other Applications of the Mobile Service*, WRC-19, Sharm el-Sheikh, Egypt, 2019.
2. Andrews, J. G., S. Buzzi, W. Choi, S. V. Hanly, A. Lozano, A. C. K. Soong, and J. C. Zhang, "What will 5G be?" *IEEE J-SAC*, Vol. 32, No. 6, 1065–1082, June 2014.
3. Rangan, S., T. S. Rappaport, and E. Erkip, "Millimeter-wave cellular wireless networks: Potentials and challenges," *Proceedings of the IEEE*, Vol. 102, No. 3, 366–385, Mar. 2014.
4. MacCartney, G. R., S. Deng, S. Sun, and T. S. Rappaport, "Millimeter-wave human blockage at 73 GHz with a simple double knife-edge diffraction model and extension for directional antennas," *Proc. IEEE VTC*, 1–6, Montreal, QC, Sept. 2016.
5. Csendes, Z. J. and P. Silvester, "Numerical solution of dielectric loaded waveguides: I-finite-element analysis," *IEEE Trans. MTT*, Vol. 18, No. 12, 1124–1131, Dec. 1970.
6. Harrington, R. F., *Field Computation by Moment Method*, Macmillan, New York, 1968.
7. Chew, W. C., J. M. Jin, E. Michielssen, and J. Song, *Fast and Efficient Algorithms in Computational Electromagnetic*, Artech House, Boston London, 2001.
8. Yee, K. S., "Numerical solution of initial boundary value problems involving Maxwell's equation in isotropic media," *IEEE Trans. AP*, Vol. 14, No. 3, 302–307, Apr. 1966.
9. Schuster, A., "An introduction to the theory of optics," *Nature*, Vol. 114, No. 2854, 48, 1924.
10. Keller, J. B., "Geometric theory of diffraction," *J.Opt.Soc.Am.*, Vol. 52, No. 2, 116–130, 1962.
11. Kouyoumjian, R. G. and P. H. Pathak, "A uniform geometrical theory of diffraction for an edge in a perfectly conducting surface," *Proc. IEEE.*, Vol. 62, No. 11, 1448–1461, Nov. 1974.
12. UFimtsev, P. Y., *Fundamentals of the Physical Theory of Diffraction*, 1–48, WILEY, Hoboken, New Jersey, 2013.
13. Kirchhoff, G., *Zur Theorie der Lichtstrahlen*, Vol. 254, No. 4, 663–695, Wiley, 1883.
14. UFimtsev, P. Y., "New insight into the classical macdonald physical optics approximation," *IEEE Antennas and Propagation Magazine*, Vol. 50, No. 3, 11–20, Jun. 2008.
15. Lam, P. T. C., S. W. Lee, and R. Acosta, "Secondary pattern computation of an arbitrarily shaped main reflector," Lewis Research Center, Cleveland, Ohio, Nov. 1984.
16. Osterman, A. and P. Ritosa, "Radio propagation calculation: A technique using 3D fresnel zones for decimeter radio waves on lidar data," *IEEE TAP*, Vol. 61, No. 6, 31–43, Dec. 2019.

17. Queiroz, A. D. C. and L. C. Trintinalia, "An analysis of human body shadowing models for ray-tracing radio channel characterization," *SBMO/IEEE MTT-S IMOC*, Porto de Galinhas, 2015.
18. Balanis, C. A., *Advanced Engineering Electromagnetics*, Chapter 6 and 7, Wiley, Hoboken, New Jersey, 2012.
19. Ludwig, A., "Computation of radiation patterns involving numerical double integration," *IEEE TAP*, Vol. 16, No. 6, 767–769, 1968.
20. Balanis, C. A., *Antenna Theory*, 620–637, WILEY, Hoboken, New Jersey, 1997.
21. Kohama, T. and M. Ando, "Localization of radiation integrals using the fresnel zone numbers," *IEICE TEE*, Vol. 95, No. 5, 928–935, 2012.
22. Yaghjian, A., "An overview of near-field antenna measurements," *IEEE TAP*, Vol. 34, No. 1, 30–45, Jan.x 1986.
23. Morita, N., N. Kumagai, and J. R. Mautz, *Integral Equation Methods for Electromagnetics*, Chapter 4, Artech House, Boston, 1990.